ISSN 1674-1056
http://cpb.iphy.ac.cn
http://iopscience.iop.org/cpb
中国物理 B
Chinese Physics
中国物理 Chinese Physics B

Ergodicity recovery of random walk in heterogeneous disordered media

Liang Luo(罗亮), Ming Yi(易鸣)
Citation: Chin. Phys. B . 2020, 29(5): 050503 . **doi:** 10.1088/1674-1056/ab8212
Journal homepage: http://cpb.iphy.ac.cn; http://iopscience.iop.org/cpb

What follows is a list of articles you may be interested in

The effect of phase fluctuation and beam splitter fluctuation on two-photon quantum random walk

Zijing Zhang(张子静), Feng Wang(王峰), Jie Song(宋杰), Yuan Zhao(赵远)
Chin. Phys. B . 2020, 29(2): 020503 . **doi:** 10.1088/1674-1056/ab6654

Nodes and layers PageRank centrality for multilayer networks

Lai-Shui Lv(吕来水), Kun Zhang(张琨), Ting Zhang(张婷), Meng-Yue Ma(麻孟越)
Chin. Phys. B . 2019, 28(2): 020501 . **doi:** 10.1088/1674-1056/28/2/020501

Uphill anomalous transport in a deterministic system with speed-dependent friction coefficient

Wei Guo(郭伟), Lu-Chun Du(杜鲁春), Zhen-Zhen Liu(刘真真), Hai Yang(杨海), Dong-Cheng Mei(梅冬成)
Chin. Phys. B . 2017, 26(1): 010502 . **doi:** 10.1088/1674-1056/26/1/010502

Anomalous transport in fluid field with random waiting time depending on the preceding jump length

Hong Zhang(张红), Guo-Hua Li(李国华)
Chin. Phys. B . 2016, 25(11): 110504 . **doi:** 10.1088/1674-1056/25/11/110504

Sub-diffusive scaling with power-law trapping times

Luo Liang, Tang Lei-Han
Chin. Phys. B . 2014, 23(7): 070514 . **doi:** 10.1088/1674-1056/23/7/070514

Ergodicity recovery of random walk in heterogeneous disordered media*

Liang Luo(罗亮)[1,2,†] and Ming Yi(易鸣)[3]

[1] Department of Physics, Huazhong Agricultural University, Wuhan 430070, China
[2] Institute of Applied Physics, Huazhong Agricultural University, Wuhan 430070, China
[3] School of Mathematics and Physics, China University of Geosciences, Wuhan 430074, China

(Received 6 February 2020; revised manuscript received 12 March 2020; accepted manuscript online 23 March 2020)

Significant and persistent trajectory-to-trajectory variance are commonly observed in particle tracking experiments, which have become a major challenge for the experimental data analysis. In this theoretical paper we investigate the ergodicity recovery behavior, which helps clarify the origin and the convergence of trajectory-to-trajectory fluctuation in various heterogeneous disordered media. The concepts of self-averaging and ergodicity are revisited in the context of trajectory analysis. The slow ergodicity recovery and the non-Gaussian diffusion in the annealed disordered media are shown as the consequences of the central limit theorem in different situations. The strange ergodicity recovery behavior is reported in the quenched disordered case, which arises from a localization mechanism. The first-passage approach is introduced to the ergodicity analysis for this case, of which the central limit theorem can be employed and the ergodicity is recovered in the length scale of diffusivity correlation.

Keywords: anomalous diffusion, random walk, disordered systems, non-Gaussian diffusion

PACS: 05.40.–a, 05.40.Fb, 66.10.C–, 87.16.dp **DOI:** 10.1088/1674-1056/ab8212

1. Introduction

Particle tracking experiments on various disordered systems, including the living cells,[1–4] colloidal[5,6] and granular[7] systems have provided numerous trajectories with rich dynamic details. This has been utilized to infer the latent dynamics of the tracer[8] and also the disordered feature of the environments,[3,9] which calls for careful statistics analysis[10,11] on random walks.

The commonly observed significant trajectory-to-trajectory variance is one of the major challenges in the trajectory analysis. Due to the stochastic nature of random walks, it exists even in the normal Brownian motion in the homogeneous media. In this simple case the fluctuation is depressed in the longer trajectories, hence the ergodicity recovers. It has been observed in experiments, however, the trajectory-to-trajectory variance can sustain in disordered media over the whole experiments,[1,2] which has been considered as a consequence of the heterogeneity of dynamics in the media. In the case of strong disorder, the heterogeneity leads to sub-diffusive continuous time random walk (CTRW).[12,13] The ergodicity would not recover in such a case.[14,15] In the case of moderate heterogeneity, one may also observe slow ergodicity recovery while the random diffusivity correlates along the trajectory. In this case the non-Gaussian diffusion has been intensively studied.[2,16–18] In recent studies on the non-Gaussian diffusion,[9,19] a localization mechanism has been discovered in the quenched disordered media with locally correlated diffusivity. The population splitting[19,20] due to the localization introduces strange and ultra-slow recovery of ergodicity. The similar behavior has also been reported in the molecular dynamics simulation.[17] It is currently unclear whether and how the ergodicity recovers in the quenched disordered case.[19,21]

In this paper, we crystalize the idea of self-averaging and ergodicity recovery by the model study in the fashion of experimental trajectory analysis, where the trap model[13,22,23] is employed as a theoretical framework containing the random walks in the homogeneous media, in the annealed disordered media with temporally correlated diffusivity, and in the quenched disordered media with spatially correlated diffusivity. One will see that the central limit theorem (CLT) plays a key role in most of the materials dealt in this paper, which is also connected to the non-Gaussian diffusion. We suggest that the first-passage time would be a proper observable for the investigation on the ergodicity recovery in the quenched disordered system.

This paper is arranged as follows. We introduce in Section 2 the concept of ergodicity in trajectories. The simple homogeneous case is revisited as an example to show in which sense we say the trajectories are similar with each other. In Section 3, we turn to the annealed disordered system. One can see how the self-averaging leads to the ergodicity recovery when the observation time is much longer than the relaxation time of the diffusivity. In Section 4, we study the more com-

*Project supported by the National Natural Science Foundation of China (Grants Nos. 11705064, 11675060, and 91730301).
†Corresponding author. E-mail: luoliang@mail.hzau.edu.cn
© 2020 Chinese Physical Society and IOP Publishing Ltd

plicated case of quenched disorder, where the self-averaging is realized by sampling large regions of the static disordered landscape. The first-passage approach is employed here. Sections 5 and 6 are the discussion and summary, respectively. The study on the non-Gaussian distribution of the displacement is shown in Appendix A and the simulation details are provided in Appendix B.

2. Ergodicity of random walk in the homogeneous media: Revisited

Let us consider the trap dynamics on a two-dimensional square lattice with lattice constant a, of which a particle jumps from site i evenly to its nearest-neighbour site j with the transition rate w. The stochastic processes can then be considered as a normal random walk on the lattice subordinated to a time series defined by the waiting time for each jump, $\{t_i\}$, where t_i follows exponential distribution

$$P(t_i = t) = 4w\exp(-4wt). \tag{1}$$

The transition rate w can be defined in different ways to model the walks in various environments. In the case of diffusion in homogeneous media, one can assign a constant w for all the jumps. The random walk turns to be the normal Brownian motion in the long time limit. In more complicated cases with heterogeneity in dynamics, w is a random variable fluctuating over time or depending on the site, which introduces anomalies such as the non-Gaussian displacement distribution and sub-diffusion. We consider in this section the homogeneous case with a constant w.

The dynamics defined above is often called the continuous time random walk in literature, which is discrete in space and continuous in time. The particle tracking experiment data is, however, in a different style that the particle positions are recorded at fixed time intervals. For better guidance to the experiment data analysis, the trajectories from the trap dynamics are discretized into the series of the particle positions $\{\boldsymbol{x}_i\}$ with the constant time interval $t_{\rm bin} = t_i - t_{i-1}$ as shown in Fig. 1. One can introduce the displacement increment

$$\xi_i = \boldsymbol{x}_i - \boldsymbol{x}_{i-1} \tag{2}$$

in each time interval. Noting that the successive jumps of CTRW have no direction correlation, i.e., $\langle \xi_i \cdot \xi_j \rangle = \delta_{ij}$ with δ_{ij} the Kronecker delta, one can see

$$\xi_i^2 \simeq n_i a^2, \quad \text{for} \quad n_i \gg 1, \tag{3}$$

where n_i is the number of the jumps in the time interval (t_{i-1}, t_i). In the homogeneous case, the jumps happen in the time scale $t_0 \sim (4w)^{-1}$. In the case that $t_{\rm bin} \gg t_0$, multiple jumps happen in one time interval and $|\xi| \gg a$. The lattice feature hence leaves the discretized trajectory. It becomes a random walk continuous in space and discrete in time.

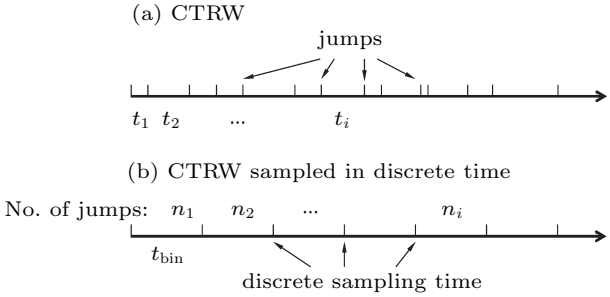


Fig. 1. (a) The time course of continuous time random walk and (b) that sampled in discrete time.

In the simulation on the homogeneous case, we are sure that the trajectories are similar due to the same and constant transition rate. It is, however, not trivial to verify the similarity of the trajectories obtained in experiments, where the underlying mechanism is usually unknown. For more rigorous analysis, one may turn to the concept of ergodicity, which refers that the observable averaged along each trajectory equals to that averaged over the ensemble of the trajectories. The most commonly used observable in the particle tracking experiments is the time-averaged mean squared displacement (TAMSD),[11,15] which is a trajectory-wise version of mean squared displacement (MSD). The TAMSD averages the square of the head-to-tail displacement of the short segments from single trajectory by

$$\overline{\delta^2}(\Delta_t, T) = \frac{1}{T-\Delta_t}\int_0^{T-\Delta_t} {\rm d}t\ \delta^2(t, \Delta_t), \tag{4}$$

where Δ_t is the time duration of the short segments, T is the duration of the long trajectory, and $\delta^2(t, \Delta_t) = |\boldsymbol{x}(t+\Delta_t) - \boldsymbol{x}(t)|^2$. In the time-discretized version,

$$\overline{\delta^2}(\Delta_t, T) = \frac{1}{M}\sum_{k=1}^{M} \delta_k^2(\Delta_t), \tag{5}$$

where

$$\delta_k(\Delta_t) = \boldsymbol{x}(t_k + \Delta_t) - \boldsymbol{x}(t_k) \tag{6}$$

is calculated for the segment initiated at time t_k, which is determined by the time lag $t_{\rm lag} = t_k - t_{k-1}$. To avoid the correlation due to the overlap of the segments, it is required that $t_{\rm lag} \geq \Delta_t$. The equality is adopted here to utilize all the frames recorded in the trajectories. There are totally $M = (T-\Delta_t)/\Delta_t$ segments sampled from the trajectory.

We estimate here the distribution of trajectory-wise TAMSD defined by Eq. (5). One may note

$$\delta_k(\Delta_t) = \sum_{i=1}^{N_{\rm q}} \xi_{k+i}, \tag{7}$$

with $N_{\rm q} = \Delta_t / t_{\rm bin}$. The squared displacement hence follows

$$\delta_k^2(\Delta_t) = \sum_{i,i'} \xi_{k+i} \cdot \xi_{k+i'} = \sum_{i=1}^{N_{\rm q}} \xi_{k+i}^2, \tag{8}$$

where $\langle \xi_i \cdot \xi_j \rangle = \delta_{ij}$ is applied for the second equality. The trajectory-wise TAMSD is then given by

$$\overline{\delta^2}(\Delta_t, T) = \frac{1}{M}\sum_{k=1}^{M}\sum_{i=1}^{N_q}\xi_{k+i}^2 = \frac{N_q}{N}\sum_{j=1}^{N}\xi_j^2 = N_q\overline{\xi^2}, \tag{9}$$

where $\overline{\xi^2}$ is the average over the trajectory and $N = Mq = (T-\Delta_t)/t_{bin}$ is roughly the number of the frames of the whole trajectory when $\Delta_t \ll T$. The problem turns to estimation of the distribution of $\overline{\xi^2}$. Since the independent jump on the lattice follows the constant rate w, the number of the jumps n_i in the time interval (t_{i-1}, t_i) follows the Poisson distribution with the expectation $n_b = 4wt_{bin}$, i.e.,

$$P(n_i = z) = \frac{{n_b}^z}{z!}\exp(-n_b). \tag{10}$$

One may note that the displacement distribution of a two-dimensional isotropic random walk of n_i steps follows the Gaussian distribution

$$P(x_i, y_i|n_i) \simeq \frac{1}{\pi n_i a^2}\exp\left(-\frac{x_i^2+y_i^2}{n_i a^2}\right), \quad \text{for} \quad n_i \gg 1. \tag{11}$$

Noting $\xi_i^2 \equiv x_i^2 + y_i^2$, we can see the following exponential distribution:

$$P(\xi_i^2 = z|n_i) = \frac{1}{n_i a^2}\exp\left(\frac{-z}{n_i a^2}\right). \tag{12}$$

From Eqs. (10) and (12), we arrive at the expectation $\langle \xi^2 \rangle = n_b a^2$, and the variance $\left\langle \left[\xi^2\right]^2 \right\rangle = \langle \xi^2 \rangle^2$. Since equation (9) shows that $\overline{\delta^2}/N_q$ is the mean value of ξ^2 of the population $N = (T-\Delta_t)/t_{bin}$. The CLT thus suggests

$$\overline{\delta^2}(\Delta_t, T)/N_q \xrightarrow{d} \mathcal{N}\left(\langle \xi^2 \rangle, \left\langle \left[\xi^2\right]^2 \right\rangle /N\right), \tag{13}$$

where $\mathcal{N}(\mu, \sigma^2)$ denotes the Gaussian distribution with the expectation μ and variance σ^2. In this case, $\mu = \langle \xi^2 \rangle$ and $\sigma^2 = \left\langle \left[\xi^2\right]^2 \right\rangle /N$. It hence gives

$$\left\langle \overline{\delta^2}(\Delta_t, T) \right\rangle = N_q \langle \xi^2 \rangle = 4wa^2\Delta_t, \tag{14}$$

$$\begin{aligned} \left\langle [\overline{\delta^2}(\Delta_t, T)]^2 \right\rangle &= N_q^2 \left\langle \left[\xi^2\right]^2 \right\rangle /N \\ &= \left(4wa^2\Delta_t\right)^2 [(T-\Delta_t)/t_{bin}]^{-1}, \end{aligned} \tag{15}$$

where $\langle \cdot \rangle$ denotes the average over trajectories. In the practice of trajectory analysis, Δ_t should be always kept much smaller than T. Otherwise one may encounter abnormal large fluctuations in TAMSD when $(T-\Delta_t) \sim t_{bin}$. $(T-\Delta_t)/t_{bin}$ is hence roughly the number of the total frames of the trajectory. One can see that the variance of $\overline{\delta^2}$ is suppressed by the self-averaging among frames in each trajectory. The mean diffusivity along each trajectory, $\overline{D} \equiv \overline{\delta^2}(\Delta_t, T)/4\Delta_t$, then converges to its ensemble expectation $\langle D \rangle = wa^2$. This is the simplest example showing how the ergodicity recovers in long random walks.

The so-called ergodicity breaking parameter[15] is introduced as the square of relative standard deviation of $\overline{\delta^2}$

$$\mathrm{EB} = \frac{\left\langle \left[\overline{\delta^2}\right]^2 - \left\langle \overline{\delta^2} \right\rangle^2 \right\rangle}{\left\langle \overline{\delta^2} \right\rangle^2}. \tag{16}$$

It has been widely employed in the trajectory analysis.[11,17,20,24] One can easily read from Eqs. (14) and (15) that $\mathrm{EB} \simeq t_{bin}/T = 1/N$ in the homogeneous case.

3. Ergodicity recovery of random walk in the annealed disordered media

In this section, we study the case that the instantaneous diffusivity fluctuates along the trajectory, which has been commonly observed in experiments. The classical CTRW[12,23,25] offers a way to capture the feature by sampling the waiting time for every jump from a non-exponential distribution $P(t)$, which has been a successful model to explain the anomalies in sub-diffusion. In the framework of trap dynamics defined above, it is equivalent to the case that the transition rate w is resampled after each jump from the distribution $P(w)$.[26]

It has been realized in recent years that the diffusivity can be a stochastic process independent of the jumps in the case with certain latent dynamics, such as the fluctuating configuration of the protein tracer or the transient interaction between the protein and the cell membrane.[8] To include this case, one may modify the classical CTRW model by introducing an additional latent dynamics, of which w is resampled from the distribution $P(w)$ by a rate $w_D = 1/t_D$. w is then correlated to the time scale t_D. When the correlation time of the diffusivity, t_D, is in a moderate scale, i.e. $\Delta_t < t_D < T$, one may observe the non-Gaussian distribution of the head-to-tail displacement $|\delta| = |\boldsymbol{x}(t+\Delta_t) - \boldsymbol{x}(t)|$ of the short segments. Noting that the latent dynamics fluctuates over time and is independent of the particle location, one can see that it is an annealed model for the non-Gaussian diffusion, which can also be understood as a lattice version of the diffusing diffusivity model introduced by Chubynsky and Slater.[27] In this section, we study the case that w follows the generalized Gamma distribution

$$P(w) = \alpha w^{\alpha-1}\exp\left(-w^\alpha\right), \tag{17}$$

where the parameter α modulates the heterogeneous level of the dynamics.[9,19,28] In the case $\alpha \to \infty$, $P(w)$ converges to a sharp peak at $w = 1$, which turns back to the homogeneous case studied in Section 2. The displacement distribution is in general non-Gaussian for $\alpha < \infty$. One can find the analysis on the non-Gaussian behavior in Appendix A.

In this annealed disordered model, the trajectory-to-trajectory variance sustains in the time scale of $\tau_{\rm D}$, which vanishes for longer observation time. Figure 2 presents 50 trajectory-wise TAMSD $\overline{\delta^2}/4\Delta_t$ for increasing observation time T. We investigate the ergodicity recovery behavior below.

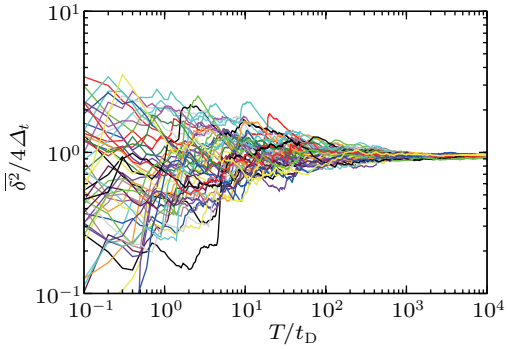


Fig. 2. The rescaled trajectory-wise TAMSD $\overline{\delta^2}/4\Delta_t$ versus the rescaled observation time $T/t_{\rm D}$ in the annealed disordered case. It contains 50 typical trajectories with $\alpha = 1.2$, $t_{\rm D} = 200$, and $\Delta_t = 16$.

One can start from Eq. (9),

$$\overline{\delta^2}(\Delta_t, T) = \frac{N_{\rm q}}{N}\sum_{j=1}^{N}\xi_j^2, \tag{18}$$

where $N = T/t_{\rm bin}$ and $N_{\rm q} = \Delta_t/t_{\rm bin}$. In the short time limit with $T < t_{\rm D}$, the diffusivity w is roughly unchanged in each concerned trajectory. The argument for Eq. (13) may also apply here, which suggests

$$\overline{\delta^2}(\Delta_t, T|w) \xrightarrow{d} \mathcal{N}\left(\mu, \sigma^2\right), \tag{19}$$

with the expectation $\mu = N_{\rm q}\left\langle\xi^2\right\rangle = 4wa^2\Delta_t$ and the variance $\sigma^2 = N_{\rm q}^2\left\langle\left[\xi^2\right]^2\right\rangle/N = (4wa^2\Delta_t)^2 t_{\rm bin}/T$. It is quite similar to Eqs. (14) and (15) in the homogeneous case, except that w is a random variable. In the $t_{\rm bin} \ll T$ limit, the distribution becomes a sharp peak around $\overline{\delta^2} = 4wa^2\Delta_t$. In the trajectory ensemble, the marginal distribution gives

$$\begin{aligned} P(\overline{\delta^2} = x) &= \int_0^\infty {\rm d}w\, P(\overline{\delta^2} = x|w)P(w) \\ &\simeq \int_0^\infty {\rm d}w\, P(w)\delta(x - 4wa^2\Delta_t). \end{aligned} \tag{20}$$

The Dirac-δ function appears in the second line. In this case, the trajectory-to-trajectory variance of $\overline{\delta^2}$ is mainly contributed by the random diffusivity w, which is highly related to the non-Gaussian diffusion discussed in Appendix A.

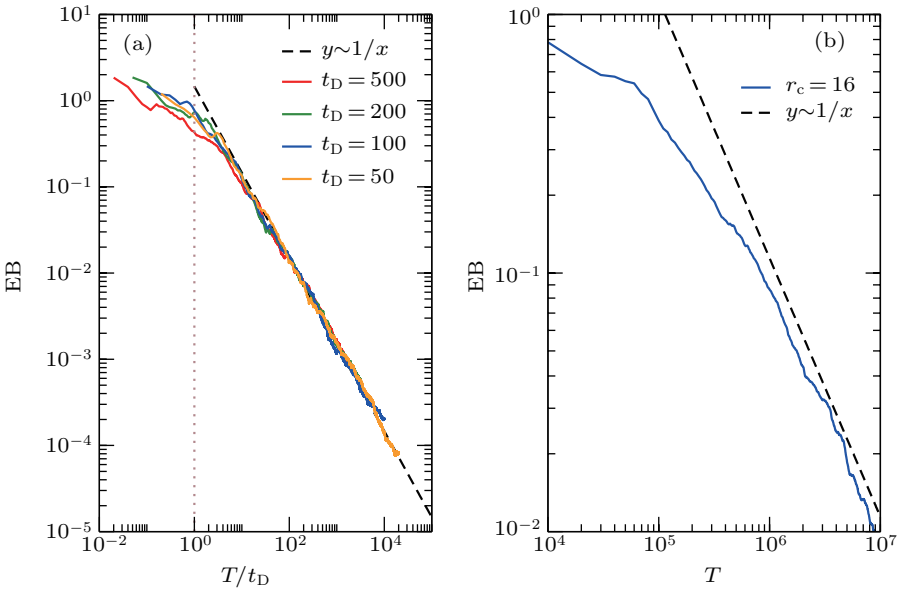


Fig. 3. The ergodicity breaking parameter in the disordered cases with $\alpha = 1.2$. (a) The annealed cases with various $t_{\rm D}$ (colored solid lines). The dash line indicates the ergodicity recovery by EB $\sim (T/t_{\rm D})^{-1}$. (b) The quenched case with $r_{\rm c} = 16$.

In the long time limit with $T \gg t_{\rm D}$, one can regroup the summation terms in Eq. (9) by the time interval $t_{\rm D}$ as

$$\overline{\delta^2}(\Delta_t, T) = \frac{N_{\rm q}}{N}\sum_{j=1}^{N_t}\delta_j^2(t_{\rm D}), \tag{21}$$

where

$$\delta_j^2(t_{\rm D}) = \sum_{i=1}^{N_{\rm p}}\xi^2_{(j-1)N_{\rm p}+i}, \tag{22}$$

with $N_{\rm p} = t_{\rm D}/t_{\rm bin}$ and $N_t = T/t_{\rm D}$. Assuming that the ξ^2 in one subgroup follows the same w, one can use again the CLT to get

$$\delta_j^2(t_{\rm D}) \xrightarrow{d} \mathcal{N}\left(\mu_j, \sigma_j^2\right), \tag{23}$$

where $\mu_j = 4w_j a^2 t_{\rm D}$ and $\sigma_j^2 = (4w_j a^2)^2 t_{\rm bin} t_{\rm D}$. $\overline{\delta^2}(\Delta_t, T)$ is then a summation over Gaussian distributed variables. One can immediately get

$$\overline{\delta^2}(\Delta_t, T) \xrightarrow{d} \mathcal{N}\left(\mu, \sigma^2\right) \tag{24}$$

with $\mu = 4a^2\Delta_t\overline{w}$ and $\sigma^2 = (4a^2\Delta_t)^2\overline{w^2}t_{\rm bin}/T$. We would like

to remind here that both $\overline{w} = \frac{1}{N_t}\sum_{j=1}^{N_t} w_j$ and $\overline{w^2} = \frac{1}{N_t}\sum_{j=1}^{N_t} w_j^2$ are random variables depending on the realization of $\{w_j\}$. In the case of $N = T/t_{\rm bin} \gg 1$, σ^2 vanishes for $T \gg t_{\rm bin}$. One can assume $\overline{\delta^2} = \mu = 4a^2\Delta_t\overline{w}$. For $N_t \gg 1$, we take the aid from the CLT again to get

$$\overline{w} \xrightarrow{d} \mathcal{N}\left(\langle w\rangle, \langle w^2\rangle/N_t\right), \tag{25}$$

where $\langle w\rangle = \int_0^\infty {\rm d}w\, wP(w)$ and $\langle w^2\rangle = \int_0^\infty {\rm d}w\, w^2P(w)$. The distribution of $\overline{\delta^2}$ is eventually obtained as

$$\overline{\delta^2} \xrightarrow{d} \mathcal{N}\left(4a^2\Delta_t\langle w\rangle, (4a^2\Delta_t)^2\langle w^2\rangle/N_t\right). \tag{26}$$

The normalized variance of $\overline{\delta^2}$ (the EB parameter) then vanishes for $T \gg t_{\rm D}$ by

$${\rm EB} = \frac{t_{\rm D}}{T}\frac{\langle w^2\rangle}{\langle w\rangle^2}, \tag{27}$$

which is confirmed by the simulation data as shown in Fig. 3(a).

4. Ergodicity recovery of random walk in the quenched disordered media

In this section, we study the random walk in the quenched disordered media, of which the diffusivity depends on the local structures of the environments. In the case that the structures relax in a quite long time scale, the local diffusivity can be assumed unchanged over the experiments. In the framework of trap dynamics, the quenched trap model (QTM)[22] assigns the random transition rates $\{w_i\}$ to sites $\{i\}$ in the lattice. In the experiment with spatial resolution high enough to reveal the local structures, the measured local diffusivity is usually correlated in the scale of the structure size. To include the locally correlated dynamics, we study the trap dynamics on the extreme landscape,[9,19] which is an extension of QTM with the locally correlated $\{w_i\}$.

The extreme landscape $\{v_i\}$ is generated by the extreme statistics as follows. First, generate the uncorrelated auxiliary potential $\{u_i\}$ following the distribution with a finite expectation and variance, such as the exponential distribution $P(u_i = u) = u_0^{-1}\exp(u/u_0)$ with $u < 0$. The local minimal value of $\{u_i\}$ is then assigned to v_i, i.e., $v_i = \min\{u_j | r_{ij} < r_{\rm c}\}$. Each minimal value controls an area of the landscape, called the "extreme basin". $\{v_i\}$ is the identity in the extreme basin, of which the radius is constrained by $r_{\rm c}$. Since v_i is the minimal value of a set of independent u_j, in the case of $r_{\rm c}^2 \gg 1$ it follows the Gumbel distribution

$$P(v_i = v) = \exp\left[v - v_0 - \exp(v - v_0)\right]. \tag{28}$$

The trap dynamics gives the transition rate as $w_i = w_0\exp(v_i/\alpha)$. Setting $w_0 = \exp(-v_0/\alpha)$, one can see that w_i follows the generalized Gamma distribution given by Eq. (17). In the low temperature case with $\alpha < 1$, the distribution of the typical waiting time $\tau_i = (4w_i)^{-1}$ is with heavy tail. Subdiffusion is then the consequence. It has been well known that the ergodicity is absent in this case.[14,15] In the $\alpha > 1$ case, the population splitting is introduced by a localization mechanism. The trajectory-to-trajectory fluctuation sustains till all the particles exit the localized state, which leads to a quite slow ergodicity recovery.

Without loss of generality, we investigate the ergodicity recovery in the quenched disordered case with $\alpha = 1.2$. Extensive simulations are performed for 160 trajectories of a quite long time ($T = 10^7$) to guarantee that the landscape is fully sampled. Figure 3(b) shows the EB parameter. It decreases quite slowly for a longer observation time T, and does not follow the EB $\sim 1/T$ rule even for a very long T. This can be more clearly illustrated by the rescaled trajectory-wise TAMSD $\overline{\delta^2}/4\Delta_t$ as shown in Fig. 4. Compared with the annealed case, the most significant feature is that the TAMSDs of some trajectories are pinned at very small values for a long time before large hops bringing them to the expected value. These TAMSDs are contributed by the trajectories initially trapped in the slowest area of the landscape. They eventually enter the mobile areas, which are remarked by the large hops. The waiting time for escaping from the slowest area couples the local diffusivity, which can span several magnitudes as shown in the figure. Noting that the diffusivity is roughly constant and hence it is strongly correlated when the particle is localized in the deepest traps, one can see that the CLT approach for independent variables is applicable only for quite large T (for the 160 simulated trajectories, $T > 10^6$).

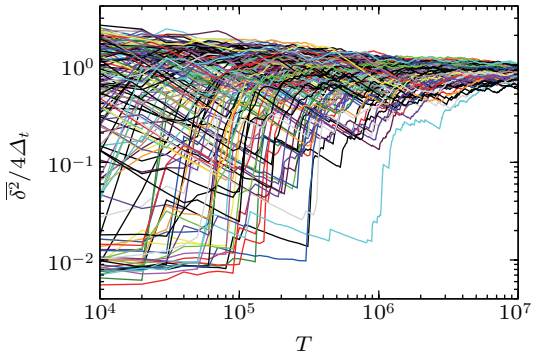


Fig. 4. The rescaled trajectory-wise TAMSD $\overline{\delta^2}/4\Delta_t$ versus the observation time T in the quenched disordered case, where $\Delta_t = 16$. It contains 160 typical trajectories on the sample with $\alpha = 1.2$, $r_{\rm c} = 16$.

To clarify the self-averaging behavior in the quenched case, one may turn to another observable, i.e., the trajectory-wise mean first-passage time (FPT). In the first-passage approach, the trajectory $\{\boldsymbol{x}(t)\}$ is divided into several segments determined by the successive first-passage events with radius r at time $\{t_k\}$. The events can be formally defined by the con-

ditions

$$|\boldsymbol{x}(t)-\boldsymbol{x}(t_k)|<r, \quad t_k<t<t_{k+1},$$
$$|\boldsymbol{x}(t_{k+1})-\boldsymbol{x}(t_k)|\geq r.$$

The first-passage time τ is then defined as $\tau_k = t_{k+1}-t_k$, which apparently depends on r. With the definitions, one can see the property of duality between the square displacement and the first-passage time. In the former one concerns the fluctuating displacements of the segments with a fixed time duration. In the later one concerns the fluctuating time durations of the segments with a fixed head-to-tail distance. The trajectory-wise mean first-passage time can be defined along a trajectory of N successive first-passage segments by

$$\overline{\tau} = \frac{1}{N}\sum_{k=1}^{N}\tau_k. \tag{29}$$

Figure 5 shows the mean first-passage time along 40 simulated trajectories. All converge to the expectation for a large N.

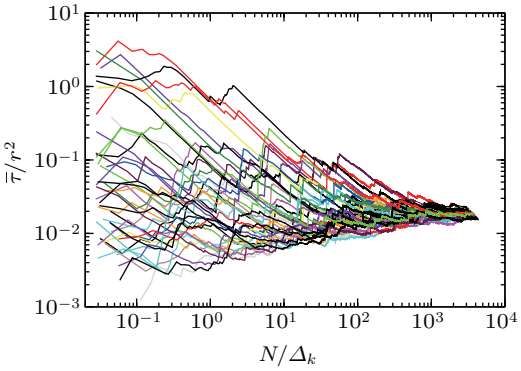


Fig. 5. The mean first-passage time of 40 trajectories on the sample with $\alpha = 1.2$, $r_c = 16$.

The trajectory-to-trajectory fluctuation can be measured by the scaled variance of $\overline{\tau}$

$$\mathrm{VT} = \frac{\langle\overline{\tau}^2\rangle - \langle\overline{\tau}\rangle^2}{\langle\overline{\tau}\rangle^2}. \tag{30}$$

One can easily see that it is the generalization of EB parameter for the first-passage approach. The CLT analysis employed in the above sections can be also applied here since the correlation in $\{\tau_k\}$ can be handled by the coarse-graining in space. One may note that the first-passage segment spans a region of radius r. The FPT τ depends only on the local diffusivity in the region. When the spanned regions of two first-passage segments denoted by k and k' do not share any site of the same extreme basin, saying, $|\boldsymbol{x}(t_{k'})-\boldsymbol{x}(t_k)|>2(r+r_c)$, τ_k and $\tau_{k'}$ are uncorrelated. Noting also $|\boldsymbol{x}(t_{k'})-\boldsymbol{x}(t_k)|^2 \simeq (k'-k)r^2$, one can see that the correlation vanishes for $\Delta_k = k'-k > 4(1+r_c/r)^2$. The CLT analysis can then be applied to the distribution of $\overline{\tau}$, which is similar to that for $\overline{\delta^2}$ in Section 3. We show the results directly here. For $N<\Delta_k$, all the summands are correlated, since the particle scans no more than one or two extreme basins. The summation would not depress the trajectory-to-trajectory fluctuation, which reflects the fluctuation of local diffusivities on different initial sites. The VT is hence kept at high level. For $N \gg \Delta_k$, the CLT suggests that it vanishes as $\mathrm{VT}\sim 1/N$. The predicted behavior is confirmed by the simulation data as shown in Fig. 6.

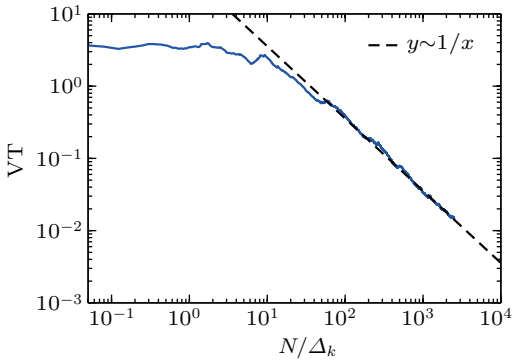


Fig. 6. The variance of the mean first-passage time of 160 simulated trajectories on the sample with $\alpha = 1.2$.

5. Discussion

Two origins of the trajectory-to-trajectory variance have been analysed in this study: the intrinsic stochastic feature of the random walk and the heterogeneity of the disordered environments, both for the annealed and quenched cases. In an ideal case, the ergodicity would eventually recover when the self-averaging over both origins is achieved in each trajectory. It is, however, the rare case in the experiments with limited observation time on the living cells. As shown in the study, the fluctuation introduced by the disordered environments persists much longer than that by the intrinsic random feature of the walk. One may expect for the long observation, the trajectory-to-trajectory variance is mainly contributed by the heterogeneity of the media. In this sense, the variance encodes the structure information of the environments. One may utilize the information and visualize the structures by the diffusion map (see Ref. [1] for example) and other ways.

This theoretical study may provide guidance on the data analysis for the particle tracking experiments on the living cells and the colloidal systems.

Living cells Due to the heterogeneity of the cellular environments, the behaviors of diffusion in different parts of the cells vary significantly.[29] The cytoplasm of eukaryotic cells is rather dynamical.[30] The nano-particles tracked in such systems are expected to follow the dynamics with fluctuating diffusivity, which has already been investigated in Section 3. Larger tracers are more likely to be entangled in the cellular structures, which are usually quasi-static over limited observation time. The quenched effect may arise in this case. The structures on the crowded cell membrane also re-

lax quite slowly, where the unique quenched effects have been reported.[2,17]

Colloidal systems In the colloidal systems, the tracer can be easily tracked and the environment structure also can be manipulated and imaged (see e.g., Ref. [5]). They are hence good proving grounds for the diffusion theories. In the dense colloidal liquids, the tracer is obstructed by the colloidal particles. Since the liquid structure changes over time, the annealed disordered model may be employed in this case. As the counterpart, the quenched effects are expected in static disordered colloidal matrices.

6. Summary

In this work, we study the ergodicity recovery of random walk in various disordered media, which concerns how the mean of the random observable converges along the elongating trajectory to its expected value. The trajectory-wise TAMSD is chosen as the observable following the convention. The ergodicity recovery in the homogeneous media is revisited in the fashion of the experimental trajectory analysis with the constraints of finite time–space resolution. It offers the first taste on how the CLT would lead to self-averaging in a series of uncorrelated random variables. In more complicated cases with the annealed dynamic heterogeneity, we have shown that the ergodicity recovers only when the observation time is much longer than the relaxation time of the temporal correlated diffusivity. In such a case, the coarse-graining in time can cancel the correlation in the summands of the TAMSD. The CLT can then be applied, which leads to the EB $\sim 1/T$ behavior.

There has been a puzzle whether and how the ergodicity recovers in the quenched disordered media, where the whole particle populations are usually split into the localized state and mobile one. In the localized state, the particle is frozen in the area with small diffusivity, which can hardly escape the area since it walks slowly. Our extensive simulation shows that the localized particles delay the ergodicity recovery for a very long time, which provides insights into the slow decay of EB parameter observed in the particle tracking experiments. It also explains the abnormal TAMSD behavior that previously observed in the molecular dynamics simulation (see Fig. 8 in Ref. [17]).

The first-passage approach is further introduced for the analysis of trajectories in the quenched disordered media, of which the trajectory is decomposed into segments of the fixed head-to-tail distance. The ergodicity recovery analysis is generalized by choosing the FPT of the segment as the observable. Since the diffusivity is locally correlated, the CLT can be applied to the mean FPT when the space scale of the trajectory is much larger than the correlation length. The variance of the mean FPT is then depressed by VT $\sim 1/L^2$, where L is the head-to-tail distance of the whole trajectory. This approach may be employed in the future analysis on the trajectories from the particle tracking experiments, especially in the case that the disordered environments are static over the experiment time scale and the particle dynamics is correlated in space but not in time.

Appendix A: The non-Gaussian displacement distribution in the annealed disordered case

In this appendix, we investigate the non-Gaussian diffusion in the annealed disordered media, of which case the ergodicity recovery has been studied in Section 3. The study on the non-Gaussian diffusion concerns the distribution of the displacement of the segments. One can start from Eqs. (2) and (6). The head-to-tail displacement of the segment is contributed by the increments via

$$\delta^{(x,y)}(\Delta_t) = \sum_{i=1}^{N_\mathrm{q}} \xi_i^{(x,y)}, \tag{A1}$$

where x or y denotes the component in the corresponding direction, and $N_\mathrm{q} = \Delta_t/t_\mathrm{bin}$. In the short time limit $\Delta_t \ll t_\mathrm{D}$, the latent variable w is roughly constant for all the increments in the segment. The uncorrelated increments $\xi = (\xi^{(x)}, \xi^{(y)})$ are identically distributed. The CLT then suggests

$$\delta^{(x,y)}(\Delta_t) \xrightarrow{d} \mathcal{N}\left(N_\mathrm{q}\left\langle \xi^{(x,y)}\right\rangle, N_\mathrm{q}\left\langle \left[\xi^{(x,y)}\right]^2\right\rangle\right), \tag{A2}$$

where $\left\langle \xi^{(x,y)}\right\rangle = 0$ and the variance $\left\langle \left[\xi^{(x,y)}\right]^2\right\rangle = 2wa^2 t_\mathrm{bin}$. The probability density function can be explicitly written in the Gaussian form

$$G(\delta^{(x,y)}, \Delta_t|w) = \frac{1}{\sqrt{4\pi w a^2 \Delta_t}} \exp\left(-\frac{\left[\delta^{(x,y)}\right]^2}{4wa^2\Delta_t}\right). \tag{A3}$$

Noting that the diffusivity w of different segments follows the distribution given by Eq. (17), the displacement distribution $P(\delta^{(x,y)}, \Delta_t)$ can be estimated as the marginal distribution

$$P(\delta^{(x,y)}, \Delta_t) = \int_0^\infty \mathrm{d}w\, G(\delta^{(x,y)}, \Delta_t|w) P(w). \tag{A4}$$

The above integral has been estimated by several approaches in previous studies,[19,28] which gives the tail behavior

$$P(\tilde{x}) \sim \frac{1}{\sqrt{2\pi}}\left(\frac{\tilde{x}^2}{2}\right)^{\frac{\alpha-1}{2(\alpha+1)}} \exp\left[-\frac{\alpha+1}{\alpha}\alpha^{\frac{1}{\alpha+1}}\left(\frac{\tilde{x}^2}{2}\right)^{\frac{\alpha}{\alpha+1}}\right], \tag{A5}$$

where $\tilde{x} = \delta^{(x,y)}/\sqrt{2wa^2\Delta_t}$. The stretched exponential tail is modulated by the roughness parameter α.

In the long time limit $\Delta_t \gg t_\mathrm{D}$, the diffusivity fluctuates in each segment. The summation in Eq. (A1) can be regrouped by the time interval t_D as

$$\delta^{(x,y)}(\Delta_t) = \sum_{j=1}^{N_\mathrm{D}} \delta_j^{(x,y)}(t_\mathrm{D}), \tag{A6}$$

where

$$\delta_j^{(x,y)}(t_{\rm D}) = \sum_{i=1}^{N_{\rm p}} \xi^{(x,y)}_{(j-1)N_{\rm p}+i}, \tag{A7}$$

$N_{\rm D} = \Delta_t/t_{\rm D}$, and $N_{\rm p} = t_{\rm D}/t_{\rm bin}$. In each subgroup, the diffusivity $w(t)$ can be assumed constant. The CLT again works as

$$\delta_j^{(x,y)}(t_{\rm D}) \xrightarrow{d} \mathcal{N}\left(0, \sigma_j^2\right), \tag{A8}$$

where the variance $\sigma_j = 2w_j a^2 t_{\rm D}$ depends on the diffusivity w_j during $(t, t+t_{\rm D})$. Their summation, $\delta^{(x,y)}(\Delta_t)$, then is also Gaussian distributed with zero mean and variance

$$\sigma^2 = \sum_{j=1}^{N_{\rm D}} \sigma_j^2 = 2a^2 t_{\rm D} \sum_{j=1}^{N_{\rm D}} w_j. \tag{A9}$$

In general, σ^2 is a variable depending on the random diffusivities w_j. In the long time limit with $N_{\rm D} \gg 1$, the summation can be approximated as $\sum_{j=1}^{N_{\rm D}} w_j \simeq N_{\rm D}\langle w\rangle$. All the $\delta^{(x,y)}(\Delta_t)$ have almost the same variance. The distribution of $\delta^{(x,y)}(\Delta_t)$ then converges to a pure Gaussian distribution

$$P(\tilde{x}) = \frac{1}{\sqrt{2\pi}} \exp\left(-\frac{\tilde{x}^2}{2}\right). \tag{A10}$$

Figure A1 depicts both Eqs. (A5) and (A10). One can see that the two limit distributions well contain the simulation results.

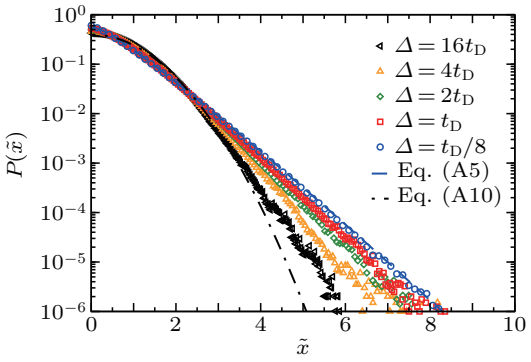


Fig. A1. The rescaled displacement distribution of the annealed model with $\alpha = 1.2$ and $t_{\rm D} = 200$. The lines show the limit distributions.

Appendix B: The simulation details

This appendix provides the details of the simulation procedure.

The trap dynamics is simulated by the Gillespie algorithm,[31] which interprets the random walk as a series of stochastic events with random time intervals. In the homogeneous case, it is composed of the jumping events on the lattice. The waiting time between two jumps is generated from the exponential distribution

$$P(\tau) = W_{\rm total} \exp(-W_{\rm total}\tau), \tag{B1}$$

where $W_{\rm total} = 4w$ is the total transition rate to the four nearest-neighboring sites. The direction of each jump is randomly chosen with even probability. w is set to 1. The trajectory is discretized as described in Section 2, where $t_{\rm bin} = 10$.

In the annealed disordered case with fluctuating diffusivity, the process is defined as a series of position and diffusivity $\{\boldsymbol{x}_i, w_i\}$. The stochastic events are then constituted by the jumps on the lattice and the diffusivity resampling from the distribution given by Eq. (17). According to the Gillespie algorithm, the waiting time between two events also follows the distribution given by Eq. (B1), while $W_{\rm total} = 4w_i + w_{\rm D}$ is the total transition rate including the jumping rate w_i and the diffusivity resampling rate $w_{\rm D}$. Each event can be either a jump to one of the neighbour sites with the probability $w_i/W_{\rm total}$ or the diffusivity resampling with the probability $w_{\rm D}/W_{\rm total}$. The typical relaxation time of the diffusivity is then given by $t_{\rm D} = 1/w_{\rm D}$.

In the quenched disordered case with spatial correlated diffusivity, the static disordered landscape is first generated by a two-step procedure shown in Section 4. The size of the disordered landscape $\{v_i\}$ is chosen as $L_x = L_y = 1024$, while the radius of the extreme basin is set as $r_{\rm c} = 16$. The periodic boundary condition is applied for a long time simulation. The initial site of each trajectory is randomly chosen following the Boltzmann distribution. The Gillespie algorithm for the random walk is similar to the case of the homogeneous case but with the site-dependent diffusivity $w_i = w_0 \exp(v_i/\alpha)$.

References

[1] Li H, Dou S X, Liu Y R, Li W, Xie P, Wang W C and Wang P Y 2015 *J. Am. Chem. Soc.* **137** 436
[2] He W, Song H, Su Y, Geng L, Ackerson B J, Peng H B and Tong P 2016 *Nat. Commun.* **7** 11701
[3] Munder M C, Midtvedt D, Franzmann T, Nuske E, Otto O, Herbig M, Ulbricht E, Müller P, Taubenberger A, Maharana S, Malinovska L, Richter D, Guck J, Zaburdev V and Alberti S 2016 *eLife* **5** e09347
[4] Li B, Dou S X, Yuan J W, Liu Y R, Li W, Ye F, Wang P Y and Li H 2018 *Proc. Natl. Acad. Sci. USA* **115** 12118
[5] Ning L, Liu P, Zong Y, Liu R, Yang M and Chen K 2019 *Phys. Rev. Lett.* **122** 178002
[6] Sentjabrskaja T, Zaccarelli E, De Michele C, Sciortino F, Tartaglia P, Voigtmann T, Egelhaaf S U and Laurati M 2016 *Nature Comm.* **7** 11133
[7] Kou B, Cao Y, Li J, Xia C, Li Z, Dong H, Zhang A, Zhang J, Kob W and Wang Y 2017 *Nature* **551** 360
[8] Manzo C, Torreno-Pina J A, Massignan P, Lapeyre Jr. G J, Lewenstein M and Garcia Parajo M F 2015 *Phys. Rev. X* **5** 011021
[9] Luo L and Yi M 2018 *Phys. Rev. E* **97** 042122
[10] Barkai E, Garini Y and Metzler R 2012 *Phys. Today* **65** 29
[11] Metzler R, Jeon J H, Cherstvy A G and Barkari E 2014 *Phys. Chem. Chem. Phys.* **16** 24128
[12] Scher H and Montroll E W 1975 *Phys. Rev. B* **12** 2455
[13] Luo L and Tang L H 2014 *Chin. Phys. B* **23** 070514
[14] Bel G and Barkai E 2005 *Phys. Rev. Lett.* **94** 240602
[15] He Y, Burov S, Metzler R and Barkai E 2008 *Phys. Rev. Lett.* **101** 058101
[16] Bae S C, Wang B, Guan J and Granick S 2009 *Proc. Natl. Acad. Sci. USA* **106** 15160
[17] Jeon J H, Javanainen M, Martinez-Seara H, Metzler R and Vattulainen I 2016 *Phys. Rev. X* **6** 021006

[18] Liu J, Li B H and Chen X S 2017 *Chin. Phys. Lett.* **34** 050201
[19] Luo L and Yi M 2019 *Phys. Rev. E* **100** 042136
[20] Cherstvy A and Metzler R 2013 *Phys. Chem. Chem. Phys.* **15** 20220
[21] Guo W, Li Y, Song W H and Du L C 2018 *J. Stat. Mech.* 033303
[22] Machta J 1981 *Phys. Rev. B* **24** 5260
[23] Haus J W and Kehr K W 1987 *Phys. Rep.* **150** 263
[24] Jeon J H, Chechkin A V and Metzler R 2014 *Phys. Chem. Chem. Phys.* **16** 15811
[25] Bouchaud J P and Georges A 1990 *Phys. Rep.* **195** 127
[26] Luo L and Tang L H 2015 *Phys. Rev. E* **92** 042137
[27] Chubynsky M V and Slater G W 2014 *Phys. Rev. Lett.* **113** 098302
[28] Sposini V, Chechkin A V, Seno F, Pagnini G and Metzler R 2018 *New J. Phys.* **20** 043044
[29] Tabaka M, Kalwarczyk T, Szymanski J, Hou S and Holyst R 2014 *Front. Phys.* **2** 54
[30] Guo M, Ehrlicher A J, Jensen M H, Renz M, Moore J R, Goldman R D, Lippincott-Schwartz J, Mackintosh F C and Weitz D A 2014 *Cell* **158** 822
[31] Gillespie D T 1977 *J. Phys. Chem.* **81** 2340